Journal of Physics: Photonics

PAPER

Single-photon generation from self-assembled GaAs/InAlAs(111)A quantum dots with ultrasmall fine-structure splitting

Christopher F Schuck[1,5], Robert Boutelle[2,5], Kevin Silverman[2], Galan Moody[3] and Paul J Simmonds[1,4,*]

[1] Micron School of Materials Science & Engineering, Boise State University, 1910 University Drive, Boise, ID 83725, United States of America
[2] National Institute of Standards and Technology, Boulder, CO 80305, United States of America
[3] Department of Electrical and Computer Engineering, University of California, Santa Barbara, Santa Barbara, CA 93106, United States of America
[4] Department of Physics, Boise State University, 1910 University Drive, Boise, ID 83725, United States of America
[5] These authors contributed equally to this work.
[*] Author to whom any correspondence should be addressed.

E-mail: paulsimmonds@boisestate.edu

Keywords: GaAs(111)A, tensile strain, single-photon emitter, quantum dots, Stranski–Krastanov

OPEN ACCESS

RECEIVED
24 December 2020

REVISED
23 February 2021

ACCEPTED FOR PUBLICATION
26 March 2021

PUBLISHED
13 April 2021

Abstract

We present a novel semiconductor single-photon source based on tensile-strained (111)-oriented GaAs/InAlAs quantum dots (QDs) exhibiting ultrasmall exciton fine-structure splitting (FSS) of ≤ 8 μeV. Using low-temperature micro-photoluminescence spectroscopy, we identify the biexciton-exciton radiative cascade from individual QDs, which, combined with small FSS, indicates these self-assembled GaAs(111) QDs are excellent candidates for polarization-entangled photon-pair generation.

1. Introduction

The polarization entanglement of photon pairs is central to certain strategies for quantum cryptography [1–3], and quantum computing [4–6]. Various methods exist for generating single or entangled photons [7–9]. These methods include nonlinear processes such as spontaneous parametric down-conversion [7, 8, 10], and emission from individual quantum emitters such as color centers [11, 12], defects in 2D materials [13], and semiconductor quantum dots (QDs) [14].

One can generate on-demand polarization entangled photons from QDs via the biexciton-exciton decay cascade [15–17]. Compared with other approaches to entangled photon generation, embedded QDs are bright [18], compact and offer the benefit of compatibility with existing planar semiconductor device architectures. The key to producing robust entanglement is for the fine-structure splitting (FSS) between the energies of the two exciton bright states to be as close to zero as possible [19]. However, these intermediate exciton states are typically non-degenerate for traditional III–V QDs such as InAs/GaAs that self-assemble on (001) surfaces. Asymmetries in (001) QD structure and piezoelectric fields create finite FSS on the order of tens or hundreds of μeV [20, 21]. Researchers have developed various techniques for tuning the FSS in an individual QD to zero, from post-growth annealing [22], to the use of external magnetic and electric fields [16, 23].

A more scalable approach would be to work with QDs for which the FSS is intrinsically zero. Due to the high symmetry of the (111) surfaces, QDs grown with this orientation should have vanishingly small FSS [21]. The challenge is that until recently, the self-assembly of (111) QDs via the Stranski–Krastanov (SK) growth mode was believed to be impossible due to the rapid relaxation of compressive strain on this surface orientation [24–27]. As a result, various alternatives have been devised to enable the growth of QDs on (111) surfaces, including surface patterning [28, 29], and approaches based on droplet epitaxy (DE) [26, 27, 30–32].

However, reports now show that the spontaneous formation of coherently strained III–V QDs on (111) surfaces is in fact possible via a modified SK growth mode, provided one uses tensile rather than compressive strain to drive the self-assembly process [33–36].

An SK-based approach to the synthesis of (111)-oriented QDs has several advantages over other methods. The SK growth mode represents a simple, single-step route to QD self-assembly without the need for complex pre- or post-growth sample processing [28, 29]. Growth of the SK QDs takes place at similar substrate temperatures to the barriers, while DE typically involves a low temperature step. Growth interrupts are hence needed immediately before and after DE to cool and heat the substrate. As well as lengthening the growth time, impurities can be incorporated at the episurface during these pauses, and rapid encapsulation of the QDs to prevent ripening effects may not be possible.

The SK growth mode permits the use of residual strain for QD band structure engineering. DE does not rely on strain as it begins with the formation of liquid metal droplets. Indeed, DE is particularly useful for forming QDs in systems such as GaAs/AlGaAs that have negligible lattice mismatch [37]. DE has been used to produce QDs in mismatched systems such as InAs/InP [27, 30, 32], or InAs/InAlAs [26], but here the InAs QDs have the larger lattice constant, resulting in compression. In contrast, it is tensile strain that drives the SK self-assembly of defect-free QDs on (111) substrates [38, 39]. We can take advantage of the tensile strain as well as the quantum confinement to modify the ground state transition energy. Unlike compressive strain which acts to widen the band gap, tensile strain narrows the band gap energy [33–35]. The tensile strain hence acts in opposition to quantum confinement, giving us highly tunable *push-pull* control over QD emission. Using tensile strain to red-shift the photon emission is compatible with efforts to generate entangled photons at fiber-optic infrared wavelengths for quantum communication [40]. What is more, tensile strain produces QDs with a light-hole valence band ground state, offering a way to convert between photon and electron qubits [41, 42].

In addition to these benefits, we have shown previously that tensile-strained GaAs/InAlAs(111)A QDs grown by SK self-assembly have naturally low FSS [33]. After surveying multiple QDs, we measured a median FSS of 7.6 μeV and demonstrated that $>$60% of these QDs have FSS $\leqslant$10 μeV, confirming the scalability of this approach. These FSS values compare favorably against the DE-based InAs QDs referred to above for which average FSS values of 17–42 μeV were reported [26, 27, 30], and are significantly lower than the 176 μeV reported by the same authors for InAs/InP(001) QDs that self-assemble via the SK growth mode [27].

Building on these promising results, in this paper we identify exciton and biexciton emission from individual GaAs/InAlAs(111)A QDs using power-dependent photoluminescence (PL), and report the first measurements of biexciton binding energy in tensile-strained GaAs(111)A QDs. We also provide the first evidence of photon antibunching in second order autocorrelation measurements, allowing us to confirm that individual GaAs(111)A QDs behave as single-photon sources.

2. Methods

Samples are grown by solid-source molecular beam epitaxy (MBE) on Fe-doped nominally on-axis ($\pm$0.5°) InP(111)A substrates. The sample structure consists of a 50 nm $In_{0.53}Ga_{0.47}As$ smoothing layer, a 200 nm $In_{0.52}Al_{0.48}As$ bottom barrier, a layer of 3.5 monolayers (MLs) GaAs QDs, a 100 nm $In_{0.52}Al_{0.48}As$ top barrier, and a 10 nm $In_{0.53}Ga_{0.47}As$ cap. The 3.5 ML GaAs QDs are grown at a substrate temperature of 540 °C, with a growth rate of 0.1 ML s^{-1}, under a V/III beam equivalent pressure ratio of 75. The lattice-matched InGaAs and InAlAs layers are grown at a substrate temperature of 510 °C, with a growth rate of 170 nm h^{-1}, under a V/III beam equivalent pressure ratio of 160. All layers are grown with As_2. We have optimized these MBE growth conditions previously [34, 36]. We calibrate substrate temperature by comparing known changes in the reflection high-energy electron diffraction (RHEED) surface reconstruction to pyrometer and thermocouple readings. We use RHEED intensity oscillations to measure growth rate, and find the beam equivalent pressure ratios with a beam flux monitor.

The ensemble PL emission spectrum from the 3.5 ML GaAs(111)A QD sample is shown in figure 1(a). We performed PL using a 633 nm continuous wave laser with the sample temperature held at 5 K in a closed-cycle cryostat. Spectra were acquired with 0.175 nm resolution by optically chopping the laser at 275 Hz, sweeping the grating of a 0.3 m monochrometer, and recording the output on a single-pixel InGaAs detector connected to a lock-in amplifier. The sharp peaks at 843 and 874 nm correspond to emission from the InAlAs barriers and the tensile-strained GaAs wetting layer, respectively [35]. Emission from the array of tensile-strained GaAs(111)A QDs gives rise to the broad PL peak centered at 1064 nm.

Atomic force microscopy (AFM) images of uncapped 3.5 ML GaAs(111)A QDs reveal an average height of 0.731 $\pm$ 0.176 nm and an average diameter of 72.4 $\pm$ 14.2 nm (figure 1(b)). These tensile-strained GaAs QDs are characteristically triangular or hexagonal in shape as a result of the threefold symmetry of the (111)

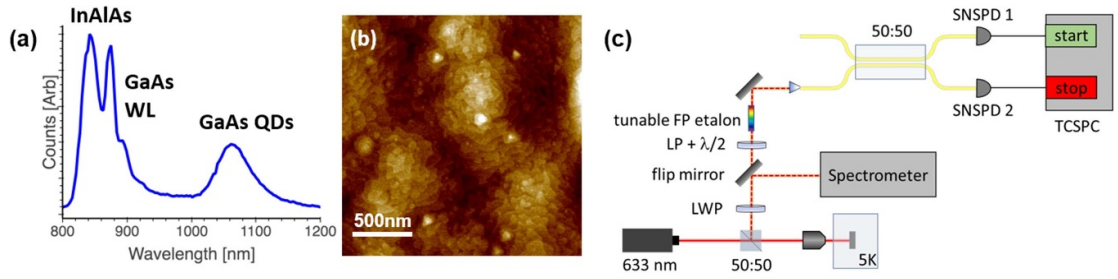

Figure 1. (a) Macro photoluminescence spectrum of 3.5 ML GaAs/InAlAs(111)A tensile-strained QDs at 5 K. Note that due to the tensile strain, the QDs emit at much longer wavelength than bulk GaAs at the same temperature (i.e. ∼815 nm). (b) 2×2 μm^2 atomic force microscope image of uncapped QDs with a 3 nm z-scale. (c) Schematic of experimental setup for macro- and micro-PL. LWP: long-wavelength pass filters; SNSPD: superconducting nanowire single-photon detector; TCSPC: time-correlated single-photon counter.

surface orientation [36]. We selected the MBE conditions above partly with the aim of producing QD arrays with very low areal density. AFM confirms a density of ∼2 μm^{-2}: around two orders of magnitude lower than is typical for traditional InAs/GaAs(001) QDs. Reducing the areal density greatly simplifies the task of collecting light from individual QDs.

To characterize the optical properties of individual QDs, we perform micro-PL (μ-PL) spectroscopy at a sample temperature of 5 K using a 633 nm continuous-wave laser for excitation (figure 1(c)). A solid-immersion lens is placed directly on the sample surface to enhance the collection efficiency, and an 18 mm aspheric lens is used to excite and collect emission from the sample. The emission is spectrally resolved with 0.07 nm resolution using the aforementioned spectrometer with a silicon charge-coupled device (CCD).

For FSS measurements, the collected μ-PL is sent through an ultra-sharp and ultra-narrow band-pass filter to isolate a single exciton resonance. The emission is next sent through a piezo-tunable Fabry–Perot etalon to map out the spectral linewidth with ∼1 GHz (∼4 μeV) resolution. A half-wave plate mounted on a rotational stage and a linear polarizer before the etalon enable measurement of the FSS as discussed in more detail below.

We acquire the second-order auto-correlation function $g^{(2)}(\tau)$ using a modified Hanbury Brown and Twiss (HBT) interferometer. The spectrometer is used as a filter to isolate emission from a single resonance with 6.9 nm bandwidth. The filtered light is coupled into a single-mode optical fiber, sent through a fiber-based 3 dB beam splitter, and single photons are detected using WSi superconducting nanowire single-photon detectors [43]. A time-correlated single-photon counting module enables measurement of $g^{(2)}(\tau)$ using a bin size of 128 ps.

3. Results and discussion

For the μ-PL measurements shown in figure 2 we intentionally selected GaAs(111)A QDs emitting in the 950 nm range, i.e. in the short wavelength tail of the main QD band centered at 1064 nm (figure 1(a)). The reasons for this are twofold. First, our Si CCD is more sensitive in this shorter wavelength range. Second, the higher density of QDs emitting close to the peak at 1064 nm makes it harder to isolate emission from individual dots for the μ-PL measurements.

Figure 2(a) shows μ-PL spectra from a representative GaAs(111)A QD at 5 K. These spectra feature two peaks at ∼957 and ∼959 nm that we assign to the exciton (X) and biexciton (XX), respectively. The linewidth of the peaks in figure 2(a) are limited by the ∼0.07 nm (∼90 μeV) resolution of the spectrometer. However from etalon data we measure linewidths of 40.0 and 81.4 μeV for the X and XX peaks, respectively. Although broader than exciton linewidths from traditional In(Ga)As(001) QDs [44, 45], those QD systems have undergone two decades of optimization, while SK-grown (111) QDs remain a comparatively recent discovery. As familiarity with the GaAs(111)A QD system grows, we will borrow from methods used over the years to reduce InAs QD linewidth. For example, we routinely use resonant pumping to reduce spectral diffusion, which is undoubtedly a big source of broadening in our QD emission [44, 45].

As we increase excitation density up to 20 μW, the intensity of both peaks increases, with the longer wavelength peak growing more quickly. We plot the peak intensities against excitation density on a log–log scale (figure 2(b)). The linear (quadratic) increase for the peak labeled X (XX) is a signature that these spectra arise from an exciton-biexciton pair confined in the same GaAs(111)A QD [46]. The exciton peak saturates

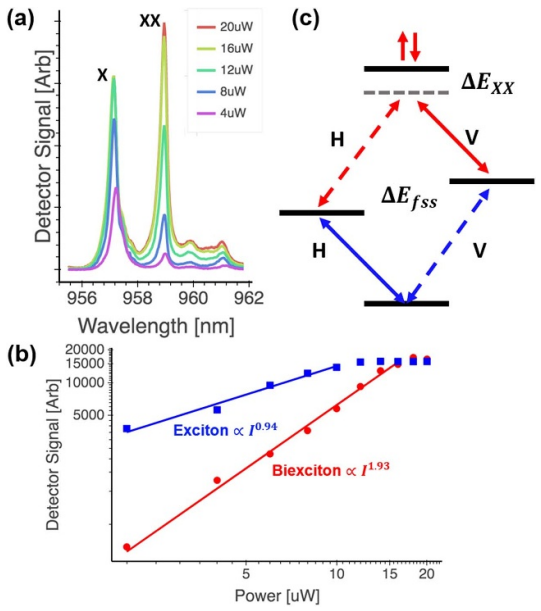

Figure 2. (a) μ-PL from an individual GaAs(111)A tensile-strained QD showing the exciton (X) and biexciton (XX) emission peaks as a function of excitation density. (b) Log–log plot of the exciton and biexciton peak intensities vs. excitation density. (c) Schematic energy level diagram showing the radiative biexciton-exciton cascade in the GaAs QDs. The exciton states are split by the FSS (ΔE_{fss}), and the biexciton is red-shifted from the unbound two-exciton state by ΔE_{XX}.

at excitation densities above $\sim$10 μW, while the biexciton intensity continues to increase quadratically until it saturates near 15 μW. We observed similar exciton-biexciton spectra across many QDs in this sample.

Notably, the biexciton-to-exciton radiative transition is red-shifted from the exciton-to-ground state transition by the biexciton binding energy $\Delta E_{XX} = 2.46$ meV. To the best of our knowledge, this is the first measurement of the biexciton binding energy in these tensile-strained, (111)-oriented QDs. The energy level structure of the exciton-biexciton decay cascade, including ΔE_{XX}, is shown schematically in figure 2(c). For emphasis, the diagram shows a large FSS between the intermediate exciton states. In QDs with an asymmetric confinement potential, such as traditional InAs/GaAs(001) QDs, the anisotropic electron–hole exchange interaction can lead to a large FSS on the order of tens or hundreds of μeV [20, 27]. As a result, photon pairs emitted through the radiative biexciton-exciton cascade are both linearly polarized either along H or V corresponding to the high symmetry directions of the crystal.

A potential advantage of the QDs studied here is the intrinsic rotational symmetry of the (111) crystal orientation [36]. This symmetry eliminates the anisotropic exchange interaction so that, in principle, the FSS vanishes [21]. To measure Δ_{fss} in the GaAs(111)A QDs, we look at the spectral linewidth of the exciton as a function of collection linear polarization angle θ. Shown in figure 3(a), the polarization-resolved μ-PL is sent through an ultrasharp bandpass filter to isolate the exciton emission and then a Fabry–Perot etalon to map out the lineshape. The emission passes through a half-wave plate and then a linear polarizer. As we rotate the half-wave plate from 0 (H) $< \theta < \pi/4$ (V), Lorentzian fits to the peaks reveal a small spectral shift of the peak center equal to $\Delta_{\text{fss}} = 8.3 \pm 0.5$ μeV. Given that the resolution of our Fabry–Perot etalon is $\sim$4 μeV, this value represents an upper bound on the measured FSS, but it is consistent with more detailed measurements of FSS in tensile-strained GaAs(111)A QDs published previously [33].

To verify the single-photon emitter behavior of the QDs, we perform an HBT experiment to measure photon-antibunching. The second-order autocorrelation function $g^{(2)}(\tau)$ is shown in figure 3(b) acquired with continuous-wave above-gap excitation. The characteristic anti-bunching dip with $g^{(2)}(\tau = 0) < 0.5$ is observed. From the fit to the data (solid black line) we extract $g^{(2)}(0) = 0.33 \pm 0.09$ and measure a recombination lifetime of $\tau_r = 0.84$ ns. From this lifetime, we estimate a maximum emission rate of 1.2 GHz, assuming perfect preparation efficiency and zero non-radiative recombination. This represents the first confirmation of single-photon emission behavior from tensile-strained QDs on a (111) surface.

A recent review of chip-scale quantum light generation allows us to put this $g^{(2)}(0)$ value into broader context with the current state-of-the-art for various single-photon technologies [9]. Although $g^{(2)}(0)$ values for defect centers of $0.1 - 0.3$ are often lower than we report here [9, 47, 48], their optical efficiencies are usually only a few percent, owing to emission in pronounced phonon sidebands [47, 48]. Compared with III–V semiconductors, the fabrication of optical cavities to enhance emission into a single optical mode, is significantly more challenging with defect center host materials like diamond. Values of $g^{(2)}(0) < 0.01$ are

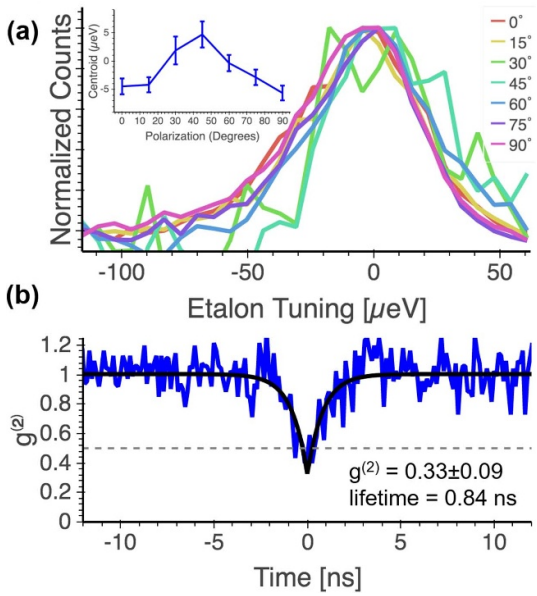

Figure 3. (a) Polarization-resolved μPL from a GaAs(111)A QD. The inset shows the measured shift in the position of the fitted PL peaks with polarization angle due to ΔE_{fss}. (b) CW pumped second-order autocorrelation of the exciton emission from an individual GaAs(111)A QD. By fitting these data we obtain $g^{(2)}(0) = 0.33 \pm 0.09$ confirming photon antibunching in these tensile-strained QDs.

typically observed from nonlinear sources [9], but they are probabilistic and thus cannot produce photons on demand, even with heralding [8]. In addition, to prevent multi-photon-pair generation events, non-linear sources are limited to lower single-photon generation rates than III–V (001) QDs. Values of $g^{(2)}(0) < 0.01$ are also routinely reported for traditional III–V (001) QDs [9, 49, 50]. However, as we have noted, SK-grown QDs with a (001) orientation typically suffer from FSS that is large enough to limit their use as entangled photon sources [20, 27].

Although (111) SK QDs are less mature than these other platforms and, so far, have higher $g^{(2)}(0)$ values, the fact that we have demonstrated single-photon anti-bunching for the first time is an exciting development. On-demand single-photon generation is not an issue for III–V (111) nanostructures [51], and we have already demonstrated that GaAs(111)A QDs exhibit low FSS [33].

We suspect that higher $g^{(2)}(0) = 0.33$ in the (111) SK QDs results from background light from the nearby wetting layer causing uncorrelated counts. To reduce $g^{(2)}(0)$ to the $<$0.01 regime and improve the single-photon purity, we intend to embed these QDs in a resonant microcavity [52, 53]. We can borrow from the more than two decades of research into (001)-oriented III–V QD nanomaterials, and apply established photonic device processing techniques to (111) QDs. A resonant microcavity could help suppress unwanted background light, whilst enhancing the collection efficiency into a single optical mode through a significant Purcell enhancement. This arrangement will also allow us to make reliable measurements of the emission rate and efficiency of these (111) SK QD single-photon sources.

Thus, we expect that through microphotonic cavity integration, these (111) SK QDs will serve as high quality, scalable sources of on-demand entangled-photon pairs, an area of future study that will build on this work.

4. Conclusions

We have explored light emission from individual GaAs(111)A QDs that self-assemble via the SK growth mode under tensile strain. Tuning the excitation density during μ-PL spectroscopy allows us to distinguish between exciton and biexciton emission, and hence to measure the biexciton binding energy. Due to their high symmetry, we demonstrate that the GaAs(111)A QDs behave as single-photon emitters, with low FSS $\leqslant$8 μeV. Tensile strain reduces the band gap of these self-assembled GaAs QDs meaning that their emission is significantly red-shifted compared with bulk GaAs. These QDs are amenable to being embedded within photonic microcavities to enhance photon collection for entanglement measurements. By using higher tensile strain or a semiconductor whose band gap is narrower than GaAs, we expect to push QD emission even further into the infrared. In this way, we anticipate that tensile-strained, (111)-oriented QDs could offer a route to entangled photon emitters compatible with telecommunications fiber optics.

Data availability statement

The data that support the findings of this study are available from the corresponding author upon reasonable request.

Acknowledgment

This material is based upon work supported by the National Science Foundation under NSF CAREER Grant No. 1555270. G M acknowledges support from AFOSR YIP Award No. FA9550-20-1-0150.

ORCID iDs

Christopher F Schuck https://orcid.org/0000-0001-7288-4560
Galan Moody https://orcid.org/0000-0002-6265-2034
Paul J Simmonds https://orcid.org/0000-0001-5524-0835

References

[1] Ekert A K 1991 *Phys. Rev. Lett.* **67** 661–3
[2] Jennewein T, Simon C, Weihs G, Weinfurter H and Zeilinger A 2000 *Phys. Rev. Lett.* **84** 4729–32
[3] O'Brien J L, Furusawa A and Vučković J 2009 *Nat. Photon.* **3** 687–95
[4] Josza R and Linden N 2003 *Proc. R. Soc.* A **459** 2011–32
[5] Vidal G 2003 *Phys. Rev. Lett.* **91** 147902
[6] Ladd T D, Jelezko F, Laflamme R, Nakamura Y, Monroe C and O'Brien J L 2010 *Nature* **464** 45–53
[7] Aharonovich I, Englund D and Toth M 2016 *Nat. Photon.* **10** 631–41
[8] Senellart P, Solomon G and White A 2017 *Nat. Nanotechnol.* **12** 1026–39
[9] Moody G, Chang L, Steiner T J and Bowers J E 2020 *AVS Quantum Sci.* **2** 041702
[10] Dada A C, Leach J, Buller G S, Padgett M J and Andersson E 2011 *Nat. Phys.* **7** 677–80
[11] Togan E *et al* 2010 *Nature* **466** 730–4
[12] Sipahigil A, Jahnke K D, Rogers L J, Teraji T, Isoya J, Zibrov A S, Jelezko F and Lukin M D 2014 *Phys. Rev. Lett.* **113** 113602
[13] Chakraborty C, Kinnischtzke L, Goodfellow K M, Beams R and Vamivakas A N 2015 *Nat. Nanotechnol.* **10** 507–11
[14] Shields A J 2007 *Nat. Photon.* **1** 215–23
[15] Benson O, Santori C, Pelton M and Yamamoto Y 2000 *Phys. Rev. Lett.* **84** 2513–16
[16] Stevenson R M, Young R J, Atkinson P, Cooper K, Ritchie D A and Shields A J 2006 *Nature* **439** 179–82
[17] Akopian N, Lindner N H, Poem E, Berlatzky Y, Avron J, Gershoni D, Gerardot B D and Petroff P M 2006 *Phys. Rev. Lett.* **96** 130501
[18] Orieux A, Versteegh M A, Jöns K D and Ducci S 2017 *Rep. Prog. Phys.* **80** 076001
[19] Hafenbrak R, Ulrich S M, Michler P, Wang L, Rastelli A and Schmidt O G 2007 *New J. Phys.* **9** 315
[20] Seguin R, Schliwa A, Rodt S, Pötschke K, Pohl U and Bimberg D 2005 *Phys. Rev. Lett.* **95** 257402
[21] Schliwa A, Winkelnkemper M, Lochmann A, Stock E and Bimberg D 2009 *Phys. Rev.* B **80** 161307(R)
[22] Young R J, Stevenson R M, Shields A J, Atkinson P, Cooper K, Ritchie D A, Groom K M, Tartakovskii A I and Skolnick M S 2005 *Phys. Rev.* B **72** 113305
[23] Gerardot B D *et al* 2007 *Appl. Phys. Lett.* **90** 041101
[24] Belk J, Sudijono J, Yamaguchi H, Zhang X, Pashley D, McConville C, Jones T and Joyce B 1997 *J. Vac. Sci. Technol.* A **15** 915
[25] Wen H, Wang Z M, Shultz J L, Liang B L and Salamo G J 2004 *Phys. Rev.* B **70** 205307
[26] Liu X *et al* 2014 *Phys. Rev.* B **90** 081301(R)
[27] Skiba-Szymanska J *et al* 2017 *Phys. Rev. Appl.* **8** 014013
[28] Dalacu D, Mnaymneh K, Lapointe J, Wu X, Poole P J, Bulgarini G, Zwiller V and Reimer M E 2012 *Nano Lett.* **12** 5919–23
[29] Juska G, Dimastrodonato V, Mereni L O, Gocalinska A and Pelucchi E 2013 *Nat. Photon.* **7** 527–31
[30] Müller T *et al* 2018 *Nat. Commun.* **9** 862
[31] Gurioli M, Wang Z, Rastelli A, Kuroda T and Sanguinetti S 2019 *Nat. Mater.* **18** 799–810
[32] Sala E M, Na Y I, Godsland M, Trapalis A and Heffernan J 2020 *Phys. Status Solidi—Rapid Res. Lett.* **14** 2000173
[33] Yerino C D *et al* 2014 *Appl. Phys. Lett.* **105** 251901
[34] Schuck C F, McCown R A, Hush A, Mello A, Roy S, Spinuzzi J W, Liang B, Huffaker D L and Simmonds P J 2018 *J. Vac. Sci. Technol.* B **36** 031803
[35] Schuck C F *et al* 2019 *Sci. Rep.* **9** 18179
[36] Schuck C F, Vallejo K D, Garrett T A, Yuan Q, Wang Y, Liang B and Simmonds P J 2020 *Semicond. Sci. Technol.* **35** 105001
[37] Watanabe K, Koguchi N and Gotoh Y 2000 *Japan. J. Appl. Phys.* **39** L79–81
[38] Simmonds P J and Lee M L 2011 *Appl. Phys. Lett.* **99** 123111
[39] Simmonds P J and Lee M L 2012 *J. Appl. Phys.* **112** 054313
[40] Ha N *et al* 2014 *Appl. Phys. Lett.* **104** 143106
[41] Vrijen R and Yablonovitch E 2001 *Physica* E **10** 569–75
[42] Huo Y H *et al* 2013 *Nat. Phys.* **10** 46–51
[43] Verma V B *et al* 2014 *Appl. Phys. Lett.* **105** 122601
[44] Berry J J, Stevens M J, Mirin R P and Silverman K L 2006 *Appl. Phys. Lett.* **88** 061114
[45] Moody G, Feng M, McDonald C, Mirin R P and Silverman K L 2014 *Phys. Rev.* B **90** 205306
[46] Matsuda K, Saiki T, Nomura S, Mihara M, Aoyagi Y, Nair S and Takagahara T 2003 *Phys. Rev. Lett.* **91** 177401

[47] Schröder T, Gädeke F, Banholzer M J and Benson O 2011 *New J. Phys.* **13** 055017
[48] Neu E, Steinmetz D, Riedrich-Möller J, Gsell S, Fischer M, Schreck M and Becher C 2011 *New J. Phys.* **13** 025012
[49] Unsleber S *et al* 2016 *Opt. Express* **24** 8539–46
[50] Arakawa Y and Holmes M J 2020 *Appl. Phys. Rev.* **7** 021309
[51] Unsleber S *et al* 2016 *Opt. Express* **24** 23198–206
[52] Wang H *et al* 2019 *Phys. Rev. Lett.* **122** 113602
[53] Ding X *et al* 2016 *Phys. Rev. Lett.* **116** 020401